FRONTIERS OF PHYSICS

RESEARCH ARTICLE
Volume 17 / Issue 6 / 63504 / 2022

Energy-resolved spin filtering effect and thermoelectric effect in topological-insulator junctions with anisotropic chiral edge states

Jia-En Yang[1], Hang Xie[2,3,†]

1 School of Electronics and IoT, Chongqing College of Electronic Engineering, Chongqing 401331, China
2 College of Physics, Chongqing University, Chongqing 401331, China
3 Chongqing Key Laboratory for Strongly-Coupled Physics, Chongqing University, Chongqing 401331, China
Corresponding author. E-mail: †xiehang2001@hotmail.com
Received March 8, 2022; accepted June 10, 2022

ABSTRACT

Topological edge states have crucial applications in the future nano spintronics devices. In this work, circularly polarized light is applied on the zigzag silicene-like nanoribbons resulting in the anisotropic chiral edge modes. An energy-dependent spin filter is designed based on the topological-insulator (TI) junctions with anisotropic chiral edge states. The resonance transmission has been observed in the TI junctions by calculating the local current distributions. And some strong Fabry–Perot resonances are found leading to the sharp transmission peaks. Whereas, the weak and asymmetric resonance corresponds to the broad transmission peaks. In addition, a qualitative relation between the resonant energy separation T_R and group velocity v_f is derived: $T_R=\pi\hbar v_f n/L$, that indicated T_R is proportional to v_f and inversely proportional to the length L of the conductor. The different T_R between the spin-up and spin-down cases results in the energy-resolved spin filtering effect. Moreover, the intensity of the circularly polarized light can modulate the group velocity v_f. Thus, the intensity of circularly polarized light, as well as the conductor-length, play very vital roles in designing the energy-dependent spin filter. Since the transmission gap root in the Fabry–Perot resonances, the thermoelectric (TE) property can be enhanced by adjusting the gap. A schedule to enhance the TE performance in the TI-junction is proposed by modulating the electric field (E_z). The TE dependence on E_z in the nanojunction is investigated, where the appropriate E_z leads to a very high spin thermopower and spin figure of merit. These TI junctions have potential usages in the nano spintronics and thermoelectric devices.

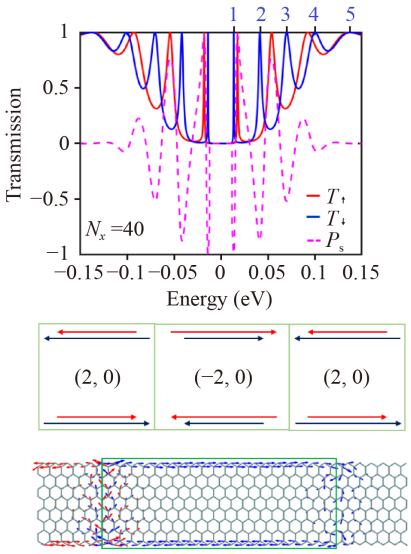

Keywords electron transport, topological edge states, 2D materials, spintronics, thermoelectric effects

1 Introduction

In recent years, two-dimensional (2D) silicene-like materials [1–5], such as silicene, germanene, stanene, and some other silicene-derived materials, have attracted extensive interest because of their unique properties. Also, the compatibility of silicene-like materials with the existing semiconductor industry has stimulated researchers to investigate its transport properties [6–13]. Compared with graphene, silicene-like materials have a

https://doi.org/10.1007/s11467-022-1189-7

strong intrinsic spin–orbit coupling (SOC) [1, 14]. The SOC is large enough to open a bulk band gap at the Dirac point making the silicene-like materials good candidates for the 2D topological insulators (2DTIs) [6, 15]. In addition, the main property of TIs is bulk-state insulation and edge-states conduction on the surface.

2DTIs include the quantum spin Hall effect (QSH), and the quantum anomalous Hall effect (QAH) [1, 14, 16, 17]. According to the bulk-edge correspondence, the QSH effect corresponds to helical edge states [18], while the QAH effect corresponds to the chiral edge state [18]. Also, the QSH state can be converted into a QAH state in the presence of circularly polarized light (CPL) [6, 18, 19]. For 2DTIs based on silicene-like materials, studies have shown that the CPL can generate the anisotropic chiral edge (ACE) modes [18, 19]. The ACE mode has the characteristics that both of the spin-up and spin-down edge states move in the same direction, but the group velocities are different [18, 19]. The topological edge states, varying with the external field, have been intensively used to design topological transistors and spin filters. For example, there have proposed some spin filters based on TI heterojunctions [6, 8, 9, 19]. One can manipulate the spin filtering property by changing the directions of the topological edge states. Zheng *et al.* [12] proposed a topological transistor based on Xenes (X = Si, Ge, or Sn) which show features of a topological insulator. By modulating the off-resonant circularly polarized light, the topological transistor can be switched between on-state and off-state. However, as far as we know, the research on energy-resolved spin filter based on TI junctions is still limited.

Traditionally, thermoelectric devices have not been widely used due to their high cost and low efficiency. The main obstacle to improve their efficiency is the interdependence between the conductance and the thermal conductivity. In analogy to the charge Seebeck effect, the ability of a thermoelectric material to convert a temperature gradient into a spin current can be measured by the spin figure of merit, which is defined $Z_sT = S_s^2|G_s|T/(K_e + K_P)$ [20]. In order to get a large quantity Z_sT, higher spin conductance G_s and thermopower S_s, but lower thermal conductance $K_e + K_p$ are required. The TIs based on silicene-materials are quite promising where the band gap opened by the strong SOC can enhance S_s. In addition, the edge modes are topologically protected against scattering while phonons are significantly scattered [20]. And it is also shown that the effect of phonon scattering effects weakens as the channel lengths of the nanodevices is longer than the mean free paths [21]. Specifically, as the width of silicene-like nanoribbons (SiNRs) decreases, the transport of edge modes remains unchanged but the lattice thermal conductance is further depressed [20, 22]. These unusual properties make the TIs suitable for high-performance thermal spintronic devices [23–26]. However, as far as we know, the thermoelectric properties of the TI based on SiNRs are less known so far.

In this work, we propose an energy-dependent spin filter with the TI junctions made from zigzag silicene-like nanoribbons (ZSiNRs). Circularly polarized light (CPL) is applied on the left/central/right region resulting in the ACE modes. We find the intensity of CPL, and the conductor length plays very vital roles in designing the spin filter nanodevices. Using the local current distributions, we also find the relationship between the resonances and peak broadening. In addition, we also show how to improve the spin thermopower and spin figure of merit by modulating the external field in the TI junctions system, which indicates promising thermoelectric applications.

2 Model and methods

The TI junctions made from the ZSiNRs consist of three parts: Lead 1, Conductor, and Lead 2 (Fig. 1). The current is incident from Lead 1 and finally transmitted into Lead 2. We use the tight-binding model for the system as below [6, 14]:

$$H = -t\sum_{\langle i,j\rangle\sigma} c_{i\sigma}^{\dagger}c_{j\sigma} + \mathrm{i}\frac{\lambda_{so}}{3\sqrt{3}}\sum_{\langle\langle i,j\rangle\rangle\sigma,\sigma'}\nu_{ij}c_{i\sigma}^{\dagger}\sigma_{\sigma\sigma'}^{z}c_{j\sigma'} + \sum_{i\sigma} elE_z\mu_i c_{i\sigma}^{\dagger}c_{i\sigma} + \mathrm{i}\frac{\lambda_{\Omega}}{3\sqrt{3}}\sum_{\langle\langle i,j\rangle\rangle\sigma}\nu_{ij}c_{i\sigma}^{\dagger}c_{j\sigma}, \quad (1)$$

where $c_{i\alpha}^{\dagger}$ and $c_{i\alpha}$ are the creation (annihilation) operator of the electron with the spin $\sigma(\sigma = \uparrow\downarrow)$ at site i; $\langle i,j\rangle$ and $\langle\langle i,j\rangle\rangle$ run over all the nearest and the next-nearest-neighbor hopping sites. The first term denotes the nearest coupling of electrons. The second term denotes the intrinsic spin–orbit interaction. In this paper, we use some silicene-like materials with $t = 1.6$ eV and $\lambda_{so} = 0.03t$ [6]. The λ_{so} value is close to that of germanene [14, 27]. The $\sigma_{\sigma\sigma'}^{z}$ is the z component of 2×2 Pauli matrix with spin indices σ and σ'. We set $v_{ij} = -1$, when the hopping is clockwise to the positive z-axis; otherwise, $v_{ij} = +1$. The third term is the potential with the staggered

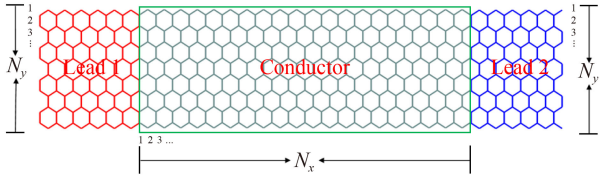

Fig. 1 Schematic diagram for the ZSiNRs-based two-terminal system. The device consists of three ZSiNRs (Lead 1, Conductor, Lead 2). The real size parameters in our study are $N_y = 16$, and N_x changes with the need of our study. The temperature gradient $\Delta T = T_L - T_R$ is applied on two leads for the thermoelectric property calculations of the TI junctions.

electric field (E_z) with $\mu_i = \pm 1$ denoting A or B sublattice, where e is the electron charge and l is the buckling thickness of ZSiNRs. The last term is the off-resonant CPL where the sign of λ_Ω depends on the right or left circulation [6, 28]. Here we note that the CPL is applied on the whole parts of the TI system. In each part of the TI junctions, there may exist different λ_Ω values, which will be detailed later.

According to the bulk-edge correspondence, specific topological phase is characterized by Chern numbers corresponds to specific topological edge states in ZSiNRs. To explore the topological phase of the silicene-like materials, we rewrite the Hamiltonian (1) as the function of the Bloch wavevector in the k-space. Then, near the K and K′ points, we approximate the Hamiltonian in the low energy range as [6, 9]

$$H_\eta^\sigma = \hbar v_F \left(\eta \tau_x k_x + \tau_y k_y\right) + \left(\eta\sigma\lambda_{so} + \eta\lambda_\Omega + elE_z\right)\tau_z, \tag{2}$$

where $v_F = \frac{\sqrt{3}at}{2}$ is the Fermi velocity with a lattice constant a, $\eta = \pm 1$ for K or K′ point (valley) and $\sigma = +1(-1)$ for spin-up (spin-down) case. $\tau = (\tau_x, \tau_y, \tau_z)$ is the Pauli matrix of the sublattice pseudospin for the A and B sites. According to Eq. (2), the spin-valley involved energy spectrum reads

$$E_{\eta\sigma} = \sqrt{\left(\hbar v_F k\right)^2 + \left(\Delta_\eta^\sigma\right)^2}. \tag{3}$$

The gap is given by $2\Delta_\eta^\sigma$, where $\Delta_\eta^\sigma = \eta\sigma\lambda_{so} + \eta\lambda_\Omega + elE_z$. The Chern number is determined by the signs of valleys and the Dirac mass: $C_{\eta\sigma} = \frac{\eta}{2} sgn\left(\Delta_\eta^\sigma\right)$ [14]. The total Chern number C and the spin Chern number C_s are defined as $C = C_\uparrow^K + C_\downarrow^K + C_\uparrow^{K'} + C_\downarrow^{K'}$ and $C_s = C_\uparrow^K + C_\uparrow^{K'} - C_\downarrow^K - C_\downarrow^{K'}$ respectively. By calculating (C, C_s), we obtain the topological phases of the corresponding edge states.

The spin-dependent transmission from lead i to lead j can be expressed as [6, 19]

$$T_{ij}^\sigma(E) = Tr\left[\boldsymbol{\Gamma}_j^\sigma(E)\boldsymbol{G}^{R,\sigma}(E)\boldsymbol{\Gamma}_i^\sigma(E)\boldsymbol{G}^{A,\sigma}(E)\right], \tag{4}$$

where $\boldsymbol{G}^{R,\sigma}(E)$ and $\boldsymbol{G}^{A,\sigma}(E)$ are the retarded and advanced Green's function with spin σ; $\boldsymbol{\Gamma}_i^\sigma(E)$ ($i = 1$ or 2) is the spin-dependent linewidth function of the lead i, which is defined as $\boldsymbol{\Gamma}_i^\sigma(E) = \mathrm{i}\left[\boldsymbol{\Sigma}_i^{R,\sigma}(E) - \boldsymbol{\Sigma}_i^{A,\sigma}(E)\right]$, where $\boldsymbol{\Sigma}_i^{R,\sigma}(E)$ and $\boldsymbol{\Sigma}_i^{A,\sigma}(E)$ are the retarded and advanced self-energy function of the lead i, respectively. The retarded (advanced) Green's function is calculated as

$$\boldsymbol{G}^{R(A),\sigma}(E) = \left[\left(E \pm \mathrm{i}\delta\right)\boldsymbol{I} - \boldsymbol{H}_C^\sigma - \sum_i \boldsymbol{\Sigma}_i^{R(A),\sigma}(E)\right]^{-1}, \tag{5}$$

where δ is a very small positive number $\boldsymbol{H}_C^\sigma$ is the Hamiltonian of the conductor, and $\boldsymbol{I}$ is the identity matrix with the conductor dimension.

The spin-dependent Seebeck coefficient (S_σ) can be derived from the spin-dependent electronic transmission probability by defining an intermediate function $L_{n\sigma}(E_\mathrm{F}, T)$ $(n = 0, 1, 2)$ as [26, 29, 30]

$$L_{n\sigma} = \frac{2}{h}\int_{-\infty}^{+\infty}\left(-\frac{\partial f}{\partial E}\right)(E - E_\mathrm{F})^n T_\sigma(E)\mathrm{d}E, \tag{6}$$

where h is the Planck constant, $f = [\exp((E - E_\mathrm{F})/K_B T) + 1]^{-1}$ is the Fermi distribution function at Fermi energy E_F with temperature T, and K_B is the Boltzmann constant. Then, one can define a spin-dependent Seebeck coefficient as S_σ

$$S_\sigma(E_\mathrm{F}) = \frac{1}{eT}\frac{L_{1\sigma}(E_\mathrm{F}, T)}{L_{0\sigma}(E_\mathrm{F}, T)}. \tag{7}$$

The spin Seebeck coefficient S_s is calculated as

$$S_\mathrm{s}(E_\mathrm{F}) = S_\uparrow - S_\downarrow. \tag{8}$$

Other spin-resolved thermoelectric coefficients (electronic conductivity G_σ and electronic thermal conductivity $K_{e\sigma}$) can be written as a function of the $L_{n\sigma}(E_\mathrm{F}, T)$:

$$G_\sigma(E_\mathrm{F}) = e^2 L_{0\sigma}(E_\mathrm{F}, T), \tag{9}$$

$$K_{e\sigma}(E_\mathrm{F}) = \frac{1}{T}[L_{2\sigma}(E_\mathrm{F},\ T) - \frac{L_{1\sigma}(E_\mathrm{F},\ T)^2}{L_{0\sigma}(E_\mathrm{F},\ T)}]. \tag{10}$$

Finally, we can define the spin conductance G_s, and the electron thermal conductance K_e of the forms $G_\mathrm{s} = G_\uparrow - G_\downarrow$, $K_e = K_{e\uparrow} + K_{e\downarrow}$, respectively. Once G_s, S_s, and K_e are known, the spin figure of merit $Z_\mathrm{s}T = S_\mathrm{s}^2|G_s|T/K_e$ can be calculated.

For the TIs, the phonon thermal conductance can be remarkably suppressed by reducing the system's width and temperature or introducing magnetic perturbations (e.g., defects or disorders) into the system [20]. Thus, in the work, as the temperature and the width of the system are chosen to be comparatively small, we neglected the phonon contribution to thermal conductance and focus our discussion on the influence of electrons.

We investigate the detailed current transport path of the TI junctions by calculating the local bond current distribution in the lead and conductor regions. The energy-dependent local bond current between site i and j is given below [8, 31, 32]:

$$J_{ij}^s(E) = H_{ji}^s G_{ij}^{<,s}(E) - G_{ji}^{<,s}(E)H_{ij}^s, \tag{11}$$

where $G^{<,s}(E)$ is the lesser Green's function in the energy domain expressed as

$$G^{<,s}(E) = -iG^{R,s}(E)\Gamma_i^s(E)G^{A,s}(E), \tag{12}$$

and H_{ij}^s is the relevant matrix element of the conductor's Hamiltonian.

3 Results and analysis

3.1 Topological phase and corresponding edge state

From the Chern number formula above, one can obtain the relation of the topological phase and external fields. We consider only the light-field term in the ZSiNRs system. One can find that if $-\lambda_{so} < \lambda_\Omega < \lambda_{so}$, the topological numbers are $(C,\ C_s) = (0,\ 1)$ or $(0,\ -1)$. This is the QSH state characterized by the locking between the spin and momentum directions of edge states, corresponding to the helical edge state [Fig. 2(a)] for the band structure and the edge state diagram. In this work, we obtain the QSH state with the $\lambda_\Omega = 0$, because the pristine silicene-like materials are a QSH insulator due to their strong SOC effect.

When $\lambda_\Omega < -\lambda_{so}$, the topological numbers are $(C,\ C_s) = (2,\ 0)$, which is a QAH state corresponding to the ACE modes. As shown in Fig. 2(b), the dispersion branches of the spin-down edge states are steeper than those of the spin-up states. Thus, the spin-down edge modes here move more quickly compared to the spin-up modes. If $\lambda_\Omega > \lambda_{so}$, the topological number are $(C,\ C_s) = (-2,\ 0)$ and the moving directions of the edge modes are reversed entirely along each edge. In addition to the moving directions, the magnitudes of the group velocities for the edge modes are also flipped. Figure 2(c) demonstrates that the spin-up edge modes are accelerated strikingly while the spin-down modes are modified slightly. These results reveal that one can modulate the edge state properties (spatial distributions and spin orientations) by adjusting the light field.

In the following section, we will show how to design the energy-resolved spin filter by combining these topological states. Furthermore, we also show how to enhance TE properties in the TI junctions system.

3.2 Energy-resolved spin filter

Now we design the energy-resolved spin filter in the two-terminal TI junctions system. In the numerical calculation, the conductor's length is first chosen as $N_x = 40$ and we mark this system by using 40-TI. Both Lead 1 and Lead 2 are set as the QAH state ($(C,\ C_s) = (2,\ 0)$) by applying the LCP light with $\lambda_\Omega = -0.15t$. And the conductor is also set as the QAH state but with $(C,\ C_s) = (-2,\ 0)$ by applying the RCP light ($\lambda_\Omega = 0.15t$). The spin-resolved transmission curves, cartoon diagram of edge state, and local current distribution are presented in Fig. 3 below.

From Fig. 3(a), there appear the Fabry–Perot resonances (FPR) [6], which gives rise to the sharp oscillations in the transmission spectrum. As can be seen, the transmittance for both spins oscillates from 0 to 1 around the Fermi energy. One can find the spin-dependent transmission peaks have symmetric line shapes and approximately the same energy separation. Moreover, the difference between the spin-up (red line) and spin-down (blue line) transmittances reveals a spin-polarized current, and the polarization is shown by a dotted line (magenta). We find that the spin filter efficiency varies from 0% through 100% around the Fermi energy. This indicates that an energy-resolved filter can be obtained in this TI junctions system. Figure 3(b) shows a cartoon diagram of the edge states in the system, and the length of the arrow is proportional to the group velocity. To show the detailed transmission mechanism in real space, the corresponding local current distributions at a specific energy ($E = 0.01373$ eV) for different spin are calculated in Fig. 3(c). The transmittance at this energy point for spin-up and spin-down is 0 and 1, respectively. For convenience, we use $n = 1$ to mark the specific energy point ($E = 0.01373$ eV) of the spin-down peak and $n = (2,\ 3,\ 4,\ 5)$ for other peaks. As illustrated in Fig. 3(c), the spin-down current (blue arrow) is strongly reflected in the lower TI edge since the edge states between the Lead 1 and the Conductor have opposite directions. Thanks to the topological protection, the reflected spin-down current flows upward along the Lead 1/Conductor boundary to the upper edge. Then it turns rightward in

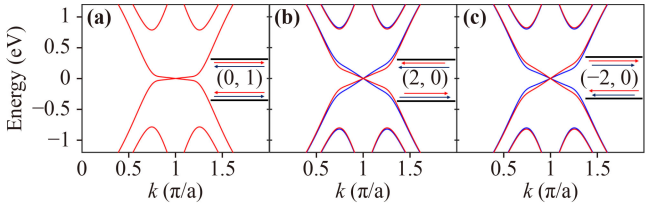

Fig. 2 Three types of TI edge states and their energy bands for ZSiNRs. **(a)** QSH state with Chern number (0, 1); **(b)** QAH state with Chern numbers (2, 0) ($\lambda_\Omega = -0.15t$); **(c)** QAH state with Chern numbers (−2, 0) ($\lambda_\Omega = 0.15t$). The red (blue) arrows or bands in the figures denote the spin-up (down) case and the red and blue bands overlap in (a). The other fixed parameters in all the cases are: $N_y = 16$, $\lambda_{so} = 0.03t$.

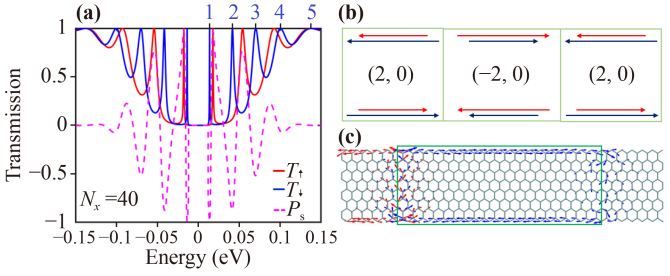

Fig. 3 **(a)** Transmission spectra from Lead 1 to Lead 2 (red: spin-up; blue: spin-down; magenta: spin-polarizability). **(b)** Cartoon diagram of the edge states in ZSiNRs-based spin filter. **(c)** Local current distribution of the spin filter around the Fermi level (at $E = 0.01373$ eV). The fixed parameters are: $N_y = 16$, $N_x = 40$, $t = 1.6$ eV, $\lambda_\Omega = 0.15t$ and $\lambda_{so} = 0.03t$.

the upper edge and flows downward along the Lead 2/Conductor boundary to the lower edge. Finally, the spin-down current turns leftward in the lower edge and the FPR current vortex forms. We notice that in the Conductor, the current loop appears very obvious due to a very strong current resonance, which seemingly results in a very small current in the lead regions. In a previous study, there have reported this result [6]. At the same time, the spin-up current (red arrow) is fully reflected. Therefore, one can obtain a perfect spin-down polarized current at this energy. All the above results show that the spin filter with energy-resolved can be obtained by applying the CPL in the ZSiNRs.

However, two detailed questions still need to be answered. First, the broadening of transmission peaks (marked by n) increases with increasing the energy, and whether these peaks correspond to the same local current distribution? Second, what is the mechanism of the different peak separations? In the next, we will have a deep discussion on these issues.

From Fig. 4 and Fig. 3(c), we see that the local current distribution varies for the different transmission peaks (n). The FPR current vortices occur when $n = 1$, 2, 3, and 4, but the resonance is weakened with increasing n value. In other words, the FPR is weakened with increasing energy. Furthermore, the current vortices disappear when $n = 5$, indicating that the peak ($n = 5$) at the higher energy is not due to the resonance. In addition, one can find obvious bulk current in the peak of $n = 5$. We believe that resonance weakened or even disappeared at higher energy is the result of the gradually strengthened bulk transport.

For the second question, one can understand it in the following way. As referred to Section 1, the QAH corresponds to the chiral edge state. Furthermore, the spin-up and spin-down have different group velocities which is an anisotropic chiral edge state (ACE) [18, 19]. From Fig. 3(b), one can find that the spin-up edge modes in Lead 1 and Lead 2 are modified moderately while in the conductor are accelerated obviously. In Lead 1 and Lead 2, the spin-down edge modes move faster than those in the conductor. Therefore, when spin-dependent current incidents from Lead 1 and eventually transmits from Lead 2, the spin-up current goes from low to high and then to low speed (the L–H–L transport process) corresponding to a large resonant separation period (T) [Fig. 3(a)], while the spin-down goes opposite process (the H–L–H transport process) with a smaller resonant period [Fig. 3(a)]. Therefore, the difference in group velocity between the leads and conductor is the essential cause of transmission splitting of the two spin cases. We will analyze this in a quantitative way below.

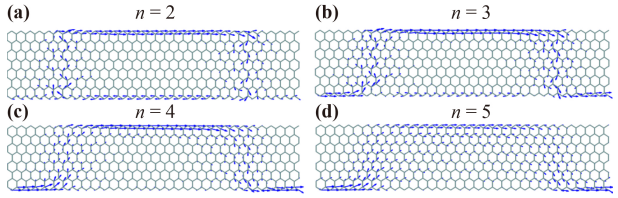

Fig. 4 Local current distribution for the TI junctions in Fig. 3 for different energy peaks **(a)** $n = 2$, **(b)** $n = 3$, **(c)** $n = 4$, and **(d)** $n = 5$ peaks.

As far as we know, previous references only obtained the relation of separation period (T_R) as $T_R = g/L$ [6, 33] in a similar TI system, where g is the state degeneracy and L is the length of the conductor. However, in this work, we find the qualitative relationship between T_R and the group velocity (v_f). One can understand it in the following way: For FPR, the electron wavelengths in two resonance peaks (λ_1 and λ_2) obey the relations $\begin{cases} n_1\lambda_1 = 2L \\ n_2\lambda_2 = 2L \end{cases}$, then we have $\frac{1}{\lambda_1} = \frac{n_1}{2L}, \frac{1}{\lambda_2} = \frac{n_2}{2L}$.

And in the gapless Dirac equation of the TI materials, $E_{1(2)} = hv_f k_{1(2)} = hv_f \frac{2\pi}{\lambda_{1(2)}}$, then $\Delta E = E_1 - E_2 = \frac{\pi h v_f n}{L}$ ($n = n_1 - n_2$). Here ΔE is nothing but T_R. Thus, the separation period is proportional to v_f and inversely proportional to L. Now we have answered the second question: the transmission splitting results from the difference in v_f of two spin electrons in the conductor (resonance) region.

In the following discussion, we will show how to control the energy-resolved spin filters by modulating the length of conductor and the light intensity.

As shown in Fig. 5, we take the conductor length and the light intensity into account. In Figs. 5(a)–(c) and Fig. 3(a), we plot the transmittance with a fixed light intensity ($\lambda_\Omega = 0.15t$) and various conductor lengths (N_x). As the conductor length increases, the peak separation (T_R) becomes smaller and the number of peaks becomes more in a certain energy range. Also, the polarization curve oscillates more rapidly near the Fermi energy. Thus, the length modulation can improve the efficiency of the energy-resolved spin filter, leading to a perfect filter at a specific energy point. Figures 5(d)–(f) and Fig. 3(a) show the transmission spectra with different light intensities. The numbers of peaks are unchanged for a fixed length, while the peak separation for two spins gets larger with increasing the light intensity. This can be explained by the formula we derived: $T_R = \frac{\pi h v_f n}{L}$. From the band calculations, we know that a larger light intensity leads to a larger group velocity, thus a larger T_R value. In addition, we find that the oscillation period of spin polarization decreases with increasing the light intensity. This is due to the large peak separation when the light intensity is raised. Therefore, one also can modulate the polarization of the spin filter by adjusting the light intensity.

3.3 Spin thermoelectric performance

The transmission gap studied in the above TI-junction

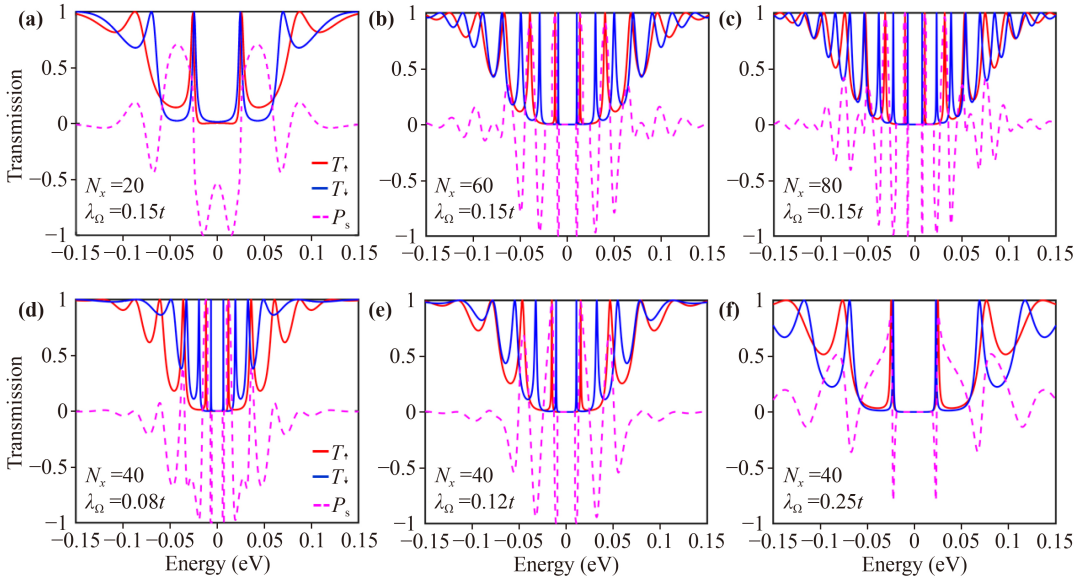

Fig. 5 **(a–c)** Transmission spectra for different lengths of conductor with a fixed light intensity: (a) 20-TI, (b) 60-TI and (c) 80-TI; **(d–f)** Transmission spectra for different light intensity with a fixed length of conductor (d) $\lambda_\Omega = 0.08t$, (e) $\lambda_\Omega = 0.12t$ and (f) $\lambda_\Omega = 0.25t$. Other fixed parameters are the same as Fig. 3.

system root in FPR. Generally speaking, the transport gap can result in a large thermopower (S_σ) and ZT [26] because of the sudden jump of the transmission coefficient near the gap edge, which is very beneficial for the thermoelectric transport. Therefore, one can expect there has a very high thermoelectric performance in these TI junctions. Figures 6(a) and (b) show the results for the spin-dependent thermopower (S_σ), spin thermopower (S_s), and spin figure of merit ($Z_\mathrm{s}T$) versus the Fermi energy, obtained from the transmission curves of Fig. 3(a) at $T = 50$ K. Figure 6(a) shows more frequent Seebeck coefficient peaks per unit energy and the sign of the thermopower can be selected by varying the Fermi energy with achievable values as high as $\pm 200\,\mu$V/K, revealing an odd function for Eq. (7). One can see that the number of transmission peaks and S_σ are the same at a given energy range. Since S_σ is relevant to the slope of T_σ at lower temperatures [34], it is obviously changed near the resonance peak due to the rapid change in T_σ. In addition, S_s has a similar variation tendency to S_σ due to $S_\mathrm{s} = S_\uparrow - S_\downarrow$. With the calculation of the electronic conductivity (G_σ) and electronic thermal conductivity ($K_{e\sigma}$) by Eqs. (9) and (10), we obtain the value of $Z_\mathrm{s}T$. Figure 6(b) shows this system has a high density of $Z_\mathrm{s}T$ peaks over a small energy range. And the value of Z_sT can achieve 0.35 at a specific energy.

Figure 7 shows the spin-dependent thermopower S_σ, spin thermopower S_s, and spin figure of merit $Z_\mathrm{s}T$ versus the Fermi energy with different electric fields (E_Z) for the 40-TI junction. From Figs. 7(a)–(c), we see that the number of thermopower peaks decreases with enhancing the E_Z value. In addition, the slope of the spin-down

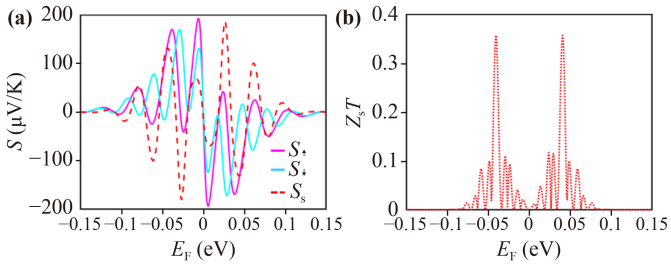

Fig. 6 **(a)** Spin-dependent thermopower (S_σ) and spin thermopower (S_s) vs. the Fermi energy (E_F); **(b)** Spin figure of merit ($Z_\mathrm{s}T$) vs. the Fermi energy E_F. The system is of 40-TI junctions with $T = 50$ K. Other parameters are the same as Fig. 3.

thermopower curve dramatically drops near zero energy, even becomes almost flat, which is different from the spin-up thermopower. One also can notice that the maximum absolute value of S_s increases with enhancing E_Z from $0.07t/(el)$ to $0.14t/(el)$, but slightly decrease with continuously enhancing E_Z from $0.14t/(el)$ to $0.16t/(el)$. The result indicates that we can obtain the optimal thermopower by applying appropriate E_Z.

These striking features of thermopower we have discussed above can be understood from the results of the corresponding transmission. As shown in Figs. 7(a2)–(c2), the number of transmission peaks decrease, and the transmission gap of spin-dependent increase with increasing the E_Z value. Thus, the decrease in the number of thermopower peaks is attributed to the reduction in the transmission peaks. We can see that the changes in the gap for spin-down electron are more

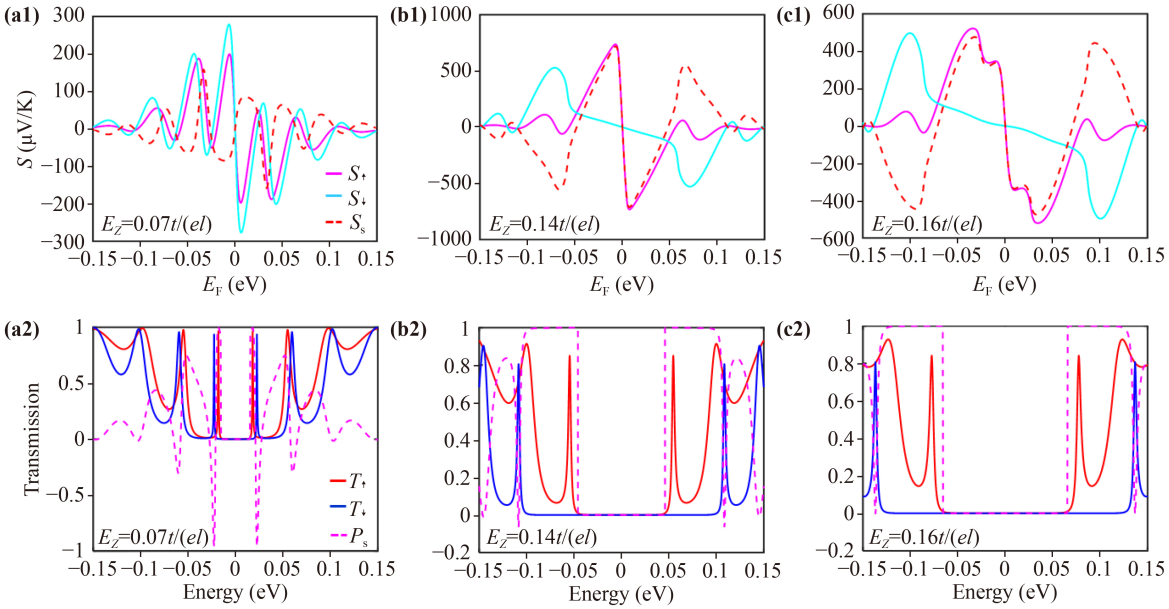

Fig. 7 **(a–c)** The dependence of spin thermopower S_s on the Fermi energy (E_F) with different electric fields (E_Z). (a1) and (a2) for $E_Z = 0.07t/(el)$; (b1) and (b2) for $E_Z = 0.14t/(el)$; (c1) and (c2) for $E_Z = 0.16t/(el)$.

pronounced than the spin-up electron, which lead to a smaller and flatter curve in the spin-down thermopower than the spin-up one near the zero energy. Thus, the maximum absolute value of S_s ($S_s = S_\uparrow - S_\downarrow$) is increased by increasing Ez.

Figure 8 shows the spin figure of merit of this system under different electric fields. As shown in the figure, the Z_sT value dramatically increases as E_Z increases, and this feature is particularly pronounced around $E_F = 0$ due to the marked increase in the spin thermopower. However, the value of Z_sT increases to maximum when $E_Z = 0.14t/(el)$. This result indicates that the TI junctions with some appropriate electric field is a favorable candidate for the high-performance thermoelectric device.

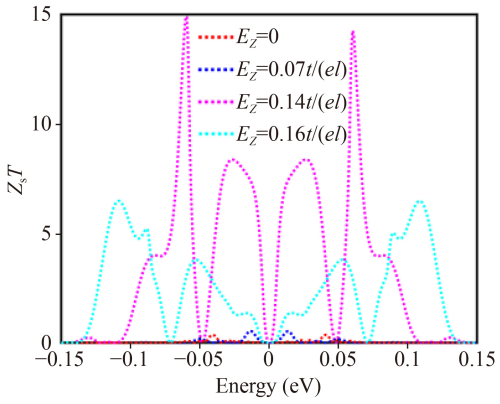

Fig. 8 The spin figure of merit (Z_sT) as a function of the Fermi energy E_F with different E_Z values for 40-TI junctions.

4 Conclusions

In summary, we use the TI hetero junctions made from the ZSiNRs to design an energy-dependent spin filter. In the TI junctions, we find that the strong FPR current vortices correspond to the sharp transmission peaks. On the contrary, the weak the resonance leads to the broad transmission peak. We also find the qualitative relationship between the resonance peak separation period (T_R) and the group velocity: the current with a higher speed in the conductor region than in the leads corresponds to a large T_R, while the current with a lower speed in the conductor has a small T_R. The different T_R between the spin-up and spin-down cases is essential for the energy-resolved spin filtering effect. We also find the intensity of CPL, as well as the conductor-length, play very vital roles in designing the energy-dependent spin filter.

In addition, we also propose to enhance the TE performance based on the resonances in the TI junctions. The mechanism is that the transmission gap can result in large S_σ and ZT values for the sudden jumps in the vicinity of the gap edge. In the TI junctions, the resonance can lead to the gap near the Fermi energy. Thus, a high spin thermopower and spin figure of merit may be achieved by applying the appropriate electric field.

Acknowledgements This work was supported by the Starting Foundation of Chongqing College of Electronic Engineering (Grant No. 120727), the National Natural Science Foundation of China (No. 11847301), the Natural Science Foundation of Chongqing (No. cstc2020jcyj-msxmX0860), and the Fundamental Research Funds for the Central Universities of China (No. 2021CDJZYJH-003).

References

1. C. C. Liu, W. X. Feng, and Y. G. Yao, Quantum spin Hall effect in silicene and two-dimensional germanium, *Phys. Rev. Lett.* 107(7), 076802 (2011)
2. C. C. Liu, H. Jiang, and Y. G. Yao, Low-energy effective Hamiltonian involving spin–orbit coupling in silicene and two-dimensional germanium and tin, *Phys. Rev. B* 84(19), 195430 (2011)
3. L. Meng, Y. L. Wang, L. Z. Zhang, S. X. Du, R. T. Wu, L. F. Li, Y. Zhang, G. Li, H. T. Zhou, W. A. Hofer, and H. J. Gao, Buckled silicene formation on Ir(111), *Nano Lett.* 13(2), 685 (2013)
4. X. C. Zhai, J. W. Gu, R. Wen, R. W. Liu, M. Zhu, X. F. Zhou, L. Y. Gong, and X. A. Li, Giant Seebeck magnetoresistance triggered by electric field and assisted by a valley through a ferromagnetic/antiferromagnetic junction in heavy group-IV monolayers, *Phys. Rev. B* 99(8), 085421 (2019)
5. C. X. Zhao and J. F. Jia, Stanene: A good platform for topological insulator and topological superconductor, *Front. Phys.* 15(5), 53201 (2020)
6. X. L. Lü and H. Xie, Spin filters and switchers in topological-insulator junctions, *Phys. Rev. Appl.* 12(6), 064040 (2019)
7. H. Y. Tian, S. K. Wang, J. G. Hu, and J. Wang, The chirality dependent spin filter design in the graphene-like junction, *J. Phys.: Condens. Matter* 27(12), 125005 (2015)
8. J. E. Yang, X. L. Lu, and H. Xie, Three-terminal spin/charge current router, *J. Phys.: Condens. Matter* 32(32), 325301 (2020)
9. J. E. Yang, X. L. Lu, C. X. Zhang, and H. Xie, Topological spin-valley filtering effects based on hybrid silicene-like nanoribbons, *New J. Phys.* 22(5), 053034 (2020)
10. X. Zhai, R. Wen, X. Zhou, W. Chen, W. Yan, L. Y. Gong, Y. Pu, and X. Li, Valley-mediated and electrically switched bipolar–unipolar transition of the spin-diode effect in heavy group-IV monolayers, *Phys. Rev. Appl.* 11(6), 064047 (2019)
11. J. Zheng, F. Chi, and Y. Guo, Spin-current diodes based on germanene and stanene subjected to local exchange fields, *Appl. Phys. Lett.* 113(11), 112404 (2018)
12. J. Zheng, Y. Xiang, C. Li, R. Yuan, F. Chi, and Y. Guo, All-optically controlled topological transistor based on Xenes, *Phys. Rev. Appl.* 14(3), 034027 (2020)
13. J. Zheng, Y. Xiang, C. Li, R. Yuan, F. Chi, and Y. Guo, Multichannel depletion-type field-effect transistor based on ferromagnetic germanene, *Phys. Rev. Appl.* 16(2), 024046 (2021)
14. M. Ezawa, Monolayer topological insulators: Silicene, germanene, and stanene, *J. Phys. Soc. Jpn.* 84(12), 121003 (2015)
15. C. C. Liu, H. Jiang, and Y. Yao, Low-energy effective Hamiltonian involving spin–orbit coupling in silicene and two-dimensional germanium and tin, *Phys. Rev. B* 84(19), 195430 (2011)
16. M. Ezawa, Valley-polarized metals and quantum anomalous Hall effect in silicene, *Phys. Rev. Lett.* 109(5), 055502 (2012)
17. H. Pan, Z. S. Li, C. C. Liu, G. B. Zhu, Z. H. Qiao, and Y. G. Yao, Valley-polarized quantum anomalous Hall effect in silicene, *Phys. Rev. Lett.* 112(10), 106802 (2014)
18. J. Mei, L. Shao, H. Xu, X. Zhu, and N. Xu, Photomodulated edge states and multiterminal transport in silicenelike nanoribbons, *Phys. Rev. B* 99(4), 045444 (2019)
19. J. E. Yang, X. L. Lü, and H. Xie, Current propagation behaviors and spin filtering effects in three-terminal topological-insulator junctions, *New J. Phys.* 22(10), 103018 (2020)
20. J. Zheng, F. Chi, and Y. Guo, Exchange and electric fields enhanced spin thermoelectric performance of germanene nano-ribbon, *J. Phys.: Condens. Matter* 27(29), 295302 (2015)
21. M. W. Chuan, M. A. Riyadi, A. Hamzah, N. E. Alias, S. Mohamed Sultan, C. S. Lim, and M. L. P. Tan, Impact of phonon scattering mechanisms on the performance of silicene nanoribbon field-effect transistors, *Results Phys.* 29, 104714 (2021)
22. X. Qi and S. Zhang, Topological insulators and superconductors, *Rev. Mod. Phys.* 83(4), 1057 (2011)
23. D. Qin, F. Pan, J. Zhou, Z. Xu, and Y. Deng, High ZT and performance controllable thermoelectric devices based on electrically gated bismuth telluride thin films, *Nano Energy* 89, 106472 (2021)
24. G. Solomon, E. Song, C. Gayner, J. A. Martinez, and Y. Amouyal, Effects of microstructure and neodymium doping on Bi_2Te_3 nanostructures: Implications for thermoelectric performance, *ACS Appl. Nano Mater.* 4(5), 4419 (2021)
25. T. H. Wang and H. T. Jeng, Topological insulator nanoribbons – A new paradigm for high thermoelectric performance, *Nano Energy* 66, 104092 (2019)
26. N. X. Yang, Q. Yan, and Q. F. Sun, Linear and nonlinear thermoelectric transport in a magnetic topological insulator nanoribbon with a domain wall, *Phys. Rev. B* 102(24), 245412 (2020)
27. X. L. Lü, Y. Xie, and H. Xie, Topological and magnetic phase transition in silicene-like zigzag nanoribbons, *New J. Phys.* 20(4), 043054 (2018)
28. K. Jatiyanon and B. Soodchomshom, Spin-valley and layer polarizations induced by topological phase transitions in bilayer silicene, *Superlatt. Microstruct.* 120, 540 (2018)
29. M. Wei, M. Zhou, B. Wang, and Y. Xing, Thermoelectric transport properties of ferromagnetic graphene with CT-invariant quantum spin Hall effect, *Phys. Rev. B* 102(7), 075432 (2020)
30. Z. Z. Yu, G. H. Xiong, and L. F. Zhang, A brief review of thermal transport in mesoscopic systems from nonequilibrium Green's function approach, *Front. Phys.*

16(4), 43201 (2021)
31. S. R. Power, M. R. Thomsen, A. P. Jauho, and T. G. Pedersen, Electron trajectories and magnetotransport in nanopatterned graphene under commensurability conditions, *Phys. Rev. B* 96(7), 075425 (2017)
32. T. Stegmann and N. Szpak, Current splitting and valley polarization in elastically deformed graphene, *2D Mater.* 6(1), 015024 (2019)
33. M. Calvo, F. de Juan, R. Ilan, E. Fox, A. Bestwick, M. Mühlbauer, J. Wang, C. Ames, P. Leubner, C. Brüne, S. C. Zhang, H. Buhmann, L. W. Molenkamp, and D. Goldhaber-Gordon, Interplay of chiral and helical states in a quantum spin Hall insulator lateral junction, *Phys. Rev. Lett.* 119(22), 226401 (2017)
34. B. Zhou, B. Zhou, X. Chen, W. Liao, and G. Zhou, Symmetry-dependent spin-charge transport and thermopower through a ZSiNR-based FM/normal/FM junction, *J. Phys.: Condens. Matter* 27(46), 465301 (2015)